AIAA JOURNAL
Vol. 44, No. 9, September 2006

Technical Notes

TECHNICAL NOTES are short manuscripts describing new developments or important results of a preliminary nature. These Notes should not exceed 2500 words (where a figure or table counts as 200 words). Following informal review by the Editors, they may be published within a few months of the date of receipt. Style requirements are the same as for regular contributions (see inside back cover).

Fast Estimation of Unsteady Flows in Turbomachinery at Multiple Interblade Phase Angles

Kivanc Ekici* and Kenneth C. Hall†
Duke University, Durham, North Carolina 27708-0300

DOI: 10.2514/1.23288

Introduction

TIME-LINEARIZED computational fluid dynamic (CFD) models for the computation of unsteady flows in turbomachinery are now used routinely in the design and analysis of turbomachinery blade rows, particularly to predict the onset of flutter. A typical flutter analysis of a rotor requires one to compute unsteady flow solutions over the full range of interblade phase angles, and hence requires significant computational time even for relatively efficient time-linearized flow solvers. Typically, one might compute the unsteady aerodynamic damping at several dozen interblade phase angles to ensure that no single interblade phase angle will flutter. In this note, we describe a fast technique that significantly reduces the computational time required to perform such a flutter clearance analysis.

In recent years, researchers have developed models to reduce the time required to compute multiple unsteady flow solutions when one or more parameters is varying. In many (but not all) cases, the varying parameter is the frequency of airfoil vibration [1,2]. For example, Florea and Hall [3] computed the dominant eigenfrequencies and mode shapes of the unsteady fluid motion within a two-dimensional cascade of airfoils using a nonsymmetric Lanczos algorithm, and then used these eigenmodes to construct a low degree-of-freedom reduced-order model of the unsteady flow field around an airfoil. Kim [4] developed a frequency-domain proper orthogonal decomposition (POD) technique and applied it to both mechanical and fluid dynamic models. Hall et al. [5] developed reduced-order models of small-disturbance unsteady flows around airfoils and turbomachinery cascades using a POD technique. Similarly, Willcox et al. [6] developed an efficient frequency-domain proper orthogonal decomposition method for low order aeroelastic control of turbomachines. Cizmas and Palacios [7] used a POD technique to construct reduced-order models to examine a turbine rotor-stator interaction problem. (For a complete review of ROM/POD methods, see Lucia et al. [8]).

In most of these investigations, the reduced-order model is constructed in such a way that estimates of the unsteady flow can be constructed rapidly over a wide range of (possibly undetermined) vibrational frequencies. In the turbomachinery flutter problem, however, because of the high mass ratio associated with turbomachinery blading, the frequency of flutter is known a priori. Instead, the interblade phase angle of flutter is not known, and one must examine all possible interblade phase angles to insure that a rotor is flutter free. This suggests that for flutter problems, reduced-order model should be constructed in which the interblade phase angle is the free parameter. One notable exception is the work of Epureanu et al. [9]. Here, a POD technique was used to form a reduced-order model of two-dimensional viscous flow based on an inviscid boundary-layer coupled flow solver. Both frequency and interblade phase angle were allowed to vary.

In this note, we present a fast technique that allows us to estimate the unsteady flows for many interblade phase angles very efficiently. Note that the base CFD solver used here is an iterative, three-dimensional time-linearized flow solver.

Methodology

The construction of the present approximate solution technique starts with a pair of three-dimensional Euler (or Navier–Stokes) flow solvers. In the time-linearized approach, one first solves for the steady flow using a conventional steady CFD solver. One then solves for the small-disturbance unsteady flow using a time-linearized (frequency domain) flow solver. This time-linearized CFD solver, through an iterative process, drives a vector of residuals $\mathbf{R}$ to zero, that is,

$$\mathbf{u}^{n+1} = \mathbf{u}^n + \mathbf{R}(\mathbf{u}^n; \bar{\mathbf{U}}, \omega, \sigma) \tag{1}$$

where n is the iteration number. Here $\mathbf{u}$ is the unknown unsteady small-disturbance solution, and $\bar{\mathbf{U}}$ is the mean background flow, previously computed using the steady CFD solver. Also, ω is the excitation frequency (e.g., the frequency of blade vibration for the flutter problem), and σ is the interblade phase angle. The residual operator can be written as a linear system given by

$$\mathbf{R} = \mathbf{A}\mathbf{u} - \mathbf{b} \tag{2}$$

where the matrix $\mathbf{A}$ and the vector $\mathbf{b}$ are functions of the mean flow, frequency, and interblade phase angle. [Here, we use an explicit Lax-Wendroff scheme [10], but the method described in this note can be applied to any scheme having the generic form given by Eq. (1).]

For flutter problems, Eq. (2) is solved using the iterative scheme [Eq. (1)] for many interblade phase angles to determine which, if any, interblade phase angles will produce destabilizing aerodynamic forces. The frequency of flutter ω, on the other hand, is usually known a priori, and for stiff rotors does not vary significantly with interblade phase angle. (For flexible disks, the approach described in this note can be used with minor modification.) We seek to reduce the computational time required to compute many such solutions.

To begin, we compute unsteady solutions for a small number M different interblade phase angles using the time-linearized CFD solver. The number of these unsteady solutions, also called snapshots, is significantly smaller than the total number of desired solutions. The snapshots are then used to form basis vectors, denoted by $\phi_1 \ldots \phi_K$ ($K \leq M$), using the proper orthogonal decomposition technique. These basis vectors will subsequently be used to compute

Received 17 February 2006; revision received 16 May 2006; accepted for publication 16 May 2006.

*Research Associate, Department of Mechanical Engineering and Materials Science. Member AIAA.

†Julian Francis Abele Professor and Chair, Department of Mechanical Engineering and Materials Science. Associate Fellow AIAA.

approximate unsteady solutions at many new interblade phase angles.

We assume that an unsteady solution for an interblade phase angle σ_{new} can be well approximated by a linear combination of the basis vectors, that is,

$$\mathbf{u}\,|_{\sigma=\sigma_{\text{new}}} \approx \mathbf{\Phi}\xi \tag{3}$$

where the columns of the matrix $\mathbf{\Phi}$ contain the basis vectors, so that

$$\mathbf{\Phi} = \begin{bmatrix} | & | & | & & | \\ \phi_1 & \phi_2 & \phi_3 & \dots & \phi_K \\ | & | & | & & | \end{bmatrix} \tag{4}$$

The vector ξ is a vector which contains the weighting coefficients associated with each basis vector.

The basis vectors are computed as follows. First, we form a matrix whose columns are the M snapshot solutions, that is,

$$\mathbf{S} = \begin{bmatrix} | & | & | & & | \\ \mathbf{u}_1 & \mathbf{u}_2 & \mathbf{u}_3 & \dots & \mathbf{u}_M \\ | & | & | & & | \end{bmatrix} \tag{5}$$

We then solve the eigenvalue problem defined by

$$\mathbf{S}^H\mathbf{S}\mathbf{v}_k = \lambda_k\mathbf{v}_k, \qquad k = 1, \dots, K \tag{6}$$

where λ_k and $\mathbf{v}_k$ are the eigenvalues and eigenvectors of the matrix $\mathbf{S}^H\mathbf{S}$. The basis vectors are then given by

$$\phi_k = \mathbf{S}\mathbf{v}_k \tag{7}$$

We pick this form for the basis vectors because, mathematically speaking, the snapshots $\mathbf{u}_m$ tend to lie in a subspace spanned by the basis vectors ϕ_k with the largest eigenvalues λ_k. Alternatively, one can also use the computed snapshots as basis vectors (without proper orthogonal decomposition), that is, $\mathbf{\Phi} = \mathbf{S}(K = M)$. However, having an orthogonal set of basis vectors results in slightly better approximate solutions using the present technique. In addition, for the results presented in this note, we have not applied order reduction, that is, we took the number of basis vectors to be equal to the number of snapshots ($K = M$).

Substituting the approximation given in Eq. (3) into Eq. (2), we have

$$\mathbf{R} = \mathbf{A}\mathbf{\Phi}\xi - \mathbf{b} \tag{8}$$

We pick the coefficients ξ so that the residual $\mathbf{R}$ projected onto the space spanned by the basis vectors is zero, that is,

$$\underbrace{\mathbf{\Phi}^H\mathbf{A}\mathbf{\Phi}}_{K\times K}\underbrace{\xi}_{K\times 1} = \underbrace{\mathbf{\Phi}^H\mathbf{b}}_{K\times 1} \tag{9}$$

Note that in Eq. (9), we need to compute the product $\mathbf{\Phi}^H\mathbf{A}\mathbf{\Phi}$. However, in the time-linearized flow solver, the matrix $\mathbf{A}$ is never computed explicitly. Instead we use the following matrix-free approach. To compute $\mathbf{A}\mathbf{\Phi}$, we set $\mathbf{u} = 0$ and run the time-linearized CFD solver for one iteration. The residual of the solver gives $\mathbf{R} = -\mathbf{b}$ [see Eq. (2)]. Next, we set $\mathbf{u} = \phi_1$, and the time-linearized CFD solver is run for one additional iteration. The matrix-vector product $\mathbf{A}\phi_1$ is obtained from the residual of the solver and the vector $\mathbf{b}$ using

$$\mathbf{A}\,\phi_1 = \mathbf{R} + \mathbf{b} \tag{10}$$

The rest of the terms, $\mathbf{A}\phi_2 \dots \mathbf{A}\phi_K$, in $\mathbf{A}\mathbf{\Phi}$ are computed in a similar fashion. Having computed $\mathbf{A}\mathbf{\Phi}$ column by column, we premultiply the result by $\mathbf{\Phi}^H$. The result is a small square matrix of size $K \times K$. Finally, we can solve for ξ from Eq. (9) using Gaussian elimination. The cost of computing ξ is approximately the cost of $K + 1$ iterations of the CFD solver (typically no more than one dozen basis vectors are used in our analysis). This should be compared with several thousand iterations per interblade phase angle using the conventional CFD solver.

The accuracy of the approximate solutions for interblade phase angles that are not members of the basis solutions depends on the number of snapshots used, and the location of the snapshots. Generally, if one uses too few snapshots (typically fewer than six), the current technique may not recover the baseline CFD solutions at all interblade phase angles. Therefore, we check the accuracy of the approximate unsteady solutions with a very simple error estimation method. Once an estimate to an unsteady solution has been obtained using the current technique, we load this solution to our CFD code and perform one iteration of the solver. Then, we check the residual of this computation giving us a direct measure of the accuracy of the solution. Generally, for our solver, a (nondimensional) residual that is less than 10^{-5} produces surface pressure distributions that are of acceptable accuracy. Furthermore, our experience has been that eight equally spaced snapshots (at every 45 deg) together with an additional snapshot in the cut-on region usually results in good approximations for all interblade phase angles.

Numerical Results

Two-Dimensional Cascade

In this section, a two-dimensional inviscid compressor is examined to validate the unsteady flow solver developed for the flutter analysis. Specifically, we consider here the middle blade row of a multistage configuration (configuration D [11]). The blades of this geometry are made up of NACA 4-digit (4.5)506 airfoils. The blades are staggered with a -49.5 deg angle and the gap-to-chord ratio is 0.8. The inlet relative Mach number and the flow angle are 0.7 and -60 deg, respectively. The nondimensional total pressure at the inlet is 2.022. In addition, the nondimensional exit static pressure is 1.797. The lengths are nondimensionalized by the aerodynamic chord of the rotor blades, velocities by the relative inflow velocity, and the pressures by the inlet dynamic pressure. The details about the mean background flow and the geometry can be found in [11,12].

The flow is assumed to be compressible and inviscid. Since the original case is two dimensional, a three-dimensional linear grid was generated by stacking the two-dimensional mesh in the radial direction. The accuracy of the baseline CFD codes (both steady and unsteady) used in this work has been previously validated (see [10,12]). Nevertheless, we compare our results presented in this note to a potential solver for completeness.

Shown in Fig. 1 is the steady pressure distribution on the blade surface obtained using the potential solver of Silkowski and Hall [11]

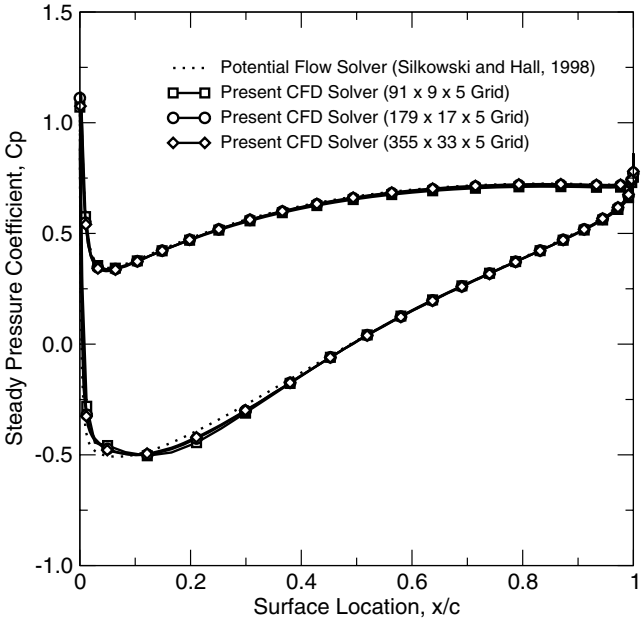

Fig. 1 Steady pressure distribution on the blade surface.

as well as our CFD code. As can be seen, the agreement with the potential solver is very good. Also shown in the same figure is the pressure distribution for different grid resolutions ($91 \times 9 \times 5$, $179 \times 17 \times 5$ and $321 \times 33 \times 5$). Overall, the agreement between different grid resolutions is very good with $91 \times 9 \times 5$ grid giving slightly different answers near the leading edge of the suction side.

For the unsteady flow problem, we assume that the rotor blades pitch around the midchord with a reduced frequency $\omega_0 c/U$ of 0.3 and an interblade phase angle of 60 deg. We first compare our unsteady CFD solver to that of Silkowski and Hall [11]. Figure 2 shows the real and imaginary parts of the unsteady pressure. Here, the unsteady pressure is nondimensionalized by $\rho U \dot{\alpha}_0 c$, where ρ and U are the density and the relative velocity at the inlet, $\dot{\alpha}_0$ is the pitching velocity of the blades and c is the chord of the blade. As in the steady case, our overall agreement to the code of Silkowski and Hall is very good. The unsteady pressure distribution for the $91 \times 9 \times 5$ grid is slightly different than the other finer grids. As a result of this grid sensitivity study, we conclude that $179 \times 17 \times 5$ grid is good enough for both steady and unsteady runs and hence we will use this grid for the rest of this case.

Next, we assume that the interblade phase angle of the vibration varies between -180 and 180 deg. For each interblade phase angle, we compute the unsteady moment coefficient C_M using the baseline CFD solver. Note the unsteady moment is nondimensionalized here by $\rho U \dot{\alpha}_0 c^2$. With this form of nondimensionalization, the aerodynamic damping is proportional to the real part of the computed unsteady moment. Therefore, for a given interblade phase

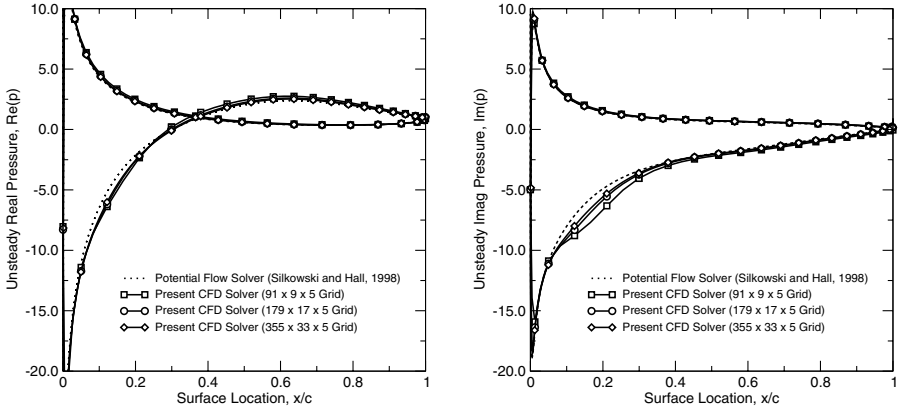

Fig. 2 Computed real and imaginary unsteady surface pressure. The rotor blades vibrate in pitch with a reduced frequency of 0.3 for 60 deg interblade phase angle.

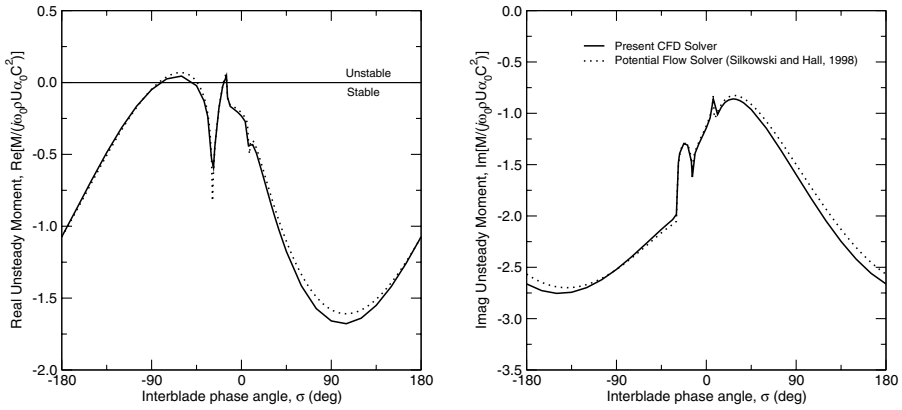

Fig. 3 Computed real and imaginary unsteady moment acting on the two-dimensional rotor blade. The rotor blades vibrate in pitch with a reduced frequency of 0.3 for a range of interblade phase angles.

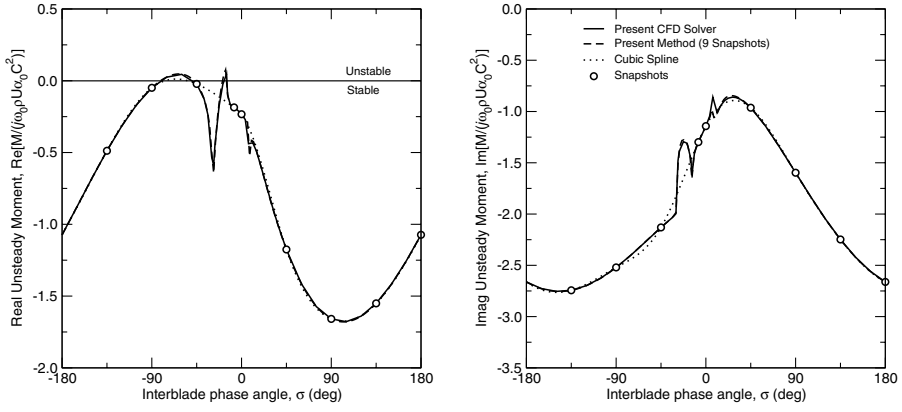

Fig. 4 Computed and estimated real and imaginary unsteady moment acting on the two-dimensional rotor blade. Nine snapshots are used for the POD method.

angle, the blades will flutter for a positive real part of the unsteady moment. Figure 3 compares the real and imaginary parts of the moment computed using the present time-linearized flow solver and the analysis of Silkowski and Hall. It can be seen that the overall agreement between the two solvers is good over the full range of interblade phase angles.

Having validated the baseline CFD solver, we now move our attention to the POD technique described in this note. The first step in the present method is to compute the unsteady flow at several interblade phase angles using the conventional time-linearized flow solver. In this example, a total of nine snapshots are computed over a range of interblade phase angles from $\sigma = -180$ deg to $+180$ deg. Eight of these snapshots are equally spaced, that is, every 45 deg, and the ninth snapshot is an arbitrarily picked interblade phase angle in the cut-on region where the waves travel unattenuated. In this case, we pick this point to be -7.5 deg. Our experience with this method has shown that including this extra point in our basis vectors greatly improves the accuracy of the present method. We then use all of these snapshots to form nine basis vectors using the POD technique described above.

Next, we compute an estimate of the unsteady solution at different interblade phase angles. Shown in Fig. 4 are the real and imaginary parts of the unsteady moment computed using the time-linearized CFD solver and the present POD method (using only nine snapshots). Also shown in the same figure are the cubic spline curves estimated using the nine basis vectors. It is clearly seen that the present method recovers the solution obtained using the time-linearized CFD solver very accurately. Especially note that, the "acoustic resonance" points are estimated accurately with the present method although none of the snapshots correspond to those interblade phase angles. Also note that although the cubic spline curve fitting does a fair job overall, it fails to predict the acoustic resonance points.

One of the important features of the present POD method is that detailed unsteady solutions for interblade phase angles that are not members of the snapshots (and basis vectors) can be estimated very accurately. Figure 5 compares the real part of the unsteady pressure contours for the computed and the estimated solutions. The interblade phase angle for this case is 60 deg, which is not a member of the nine snapshot solutions. The differences in the contour plots are indistinguishable, again confirming the accuracy of the present method.

Next, we investigate the effect of the number of snapshots used in the POD method. We first computed basis vectors using seven, nine,

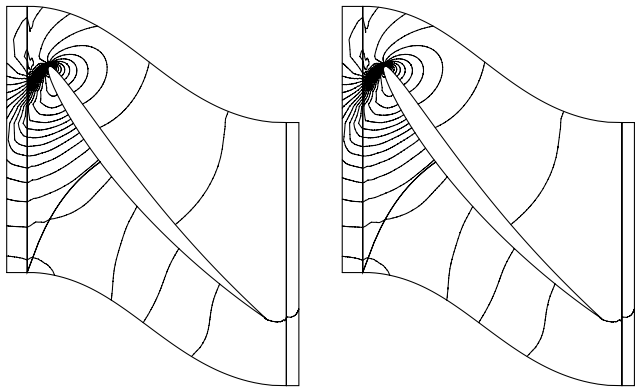

a) Time-linearized CFD solution **b) Estimated solution using the POD technique**

Fig. 5 Real part of computed and estimated unsteady pressure contours.

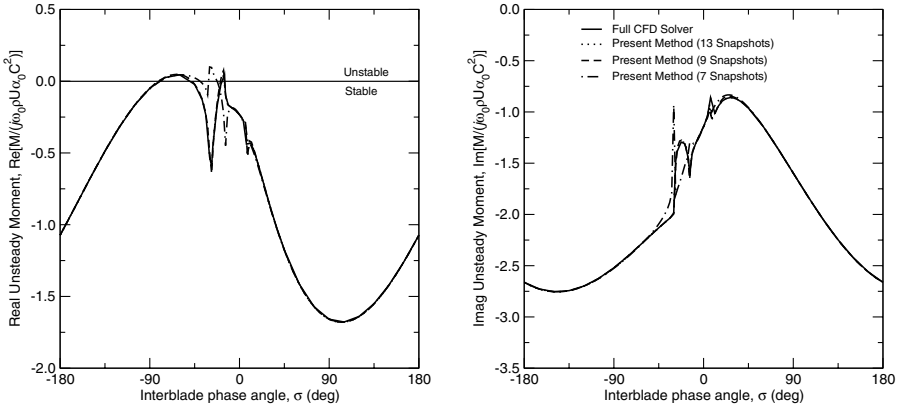

Fig. 6 Real and imaginary unsteady moment acting on the two-dimensional rotor blade for the full time-linearized CFD computation and the present POD method. The blades vibrate in pitch with a reduced frequency of 0.3.

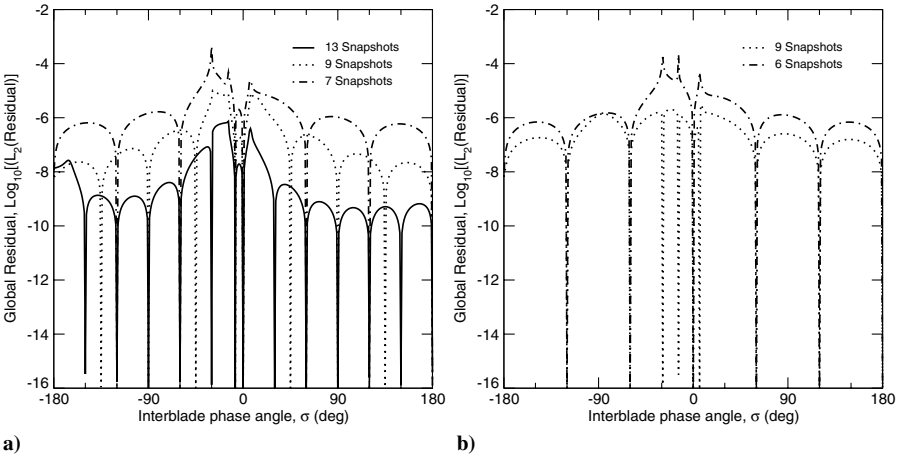

a) **b)**

Fig. 7 Residuals of the estimated solutions on the blade surface for the present method.

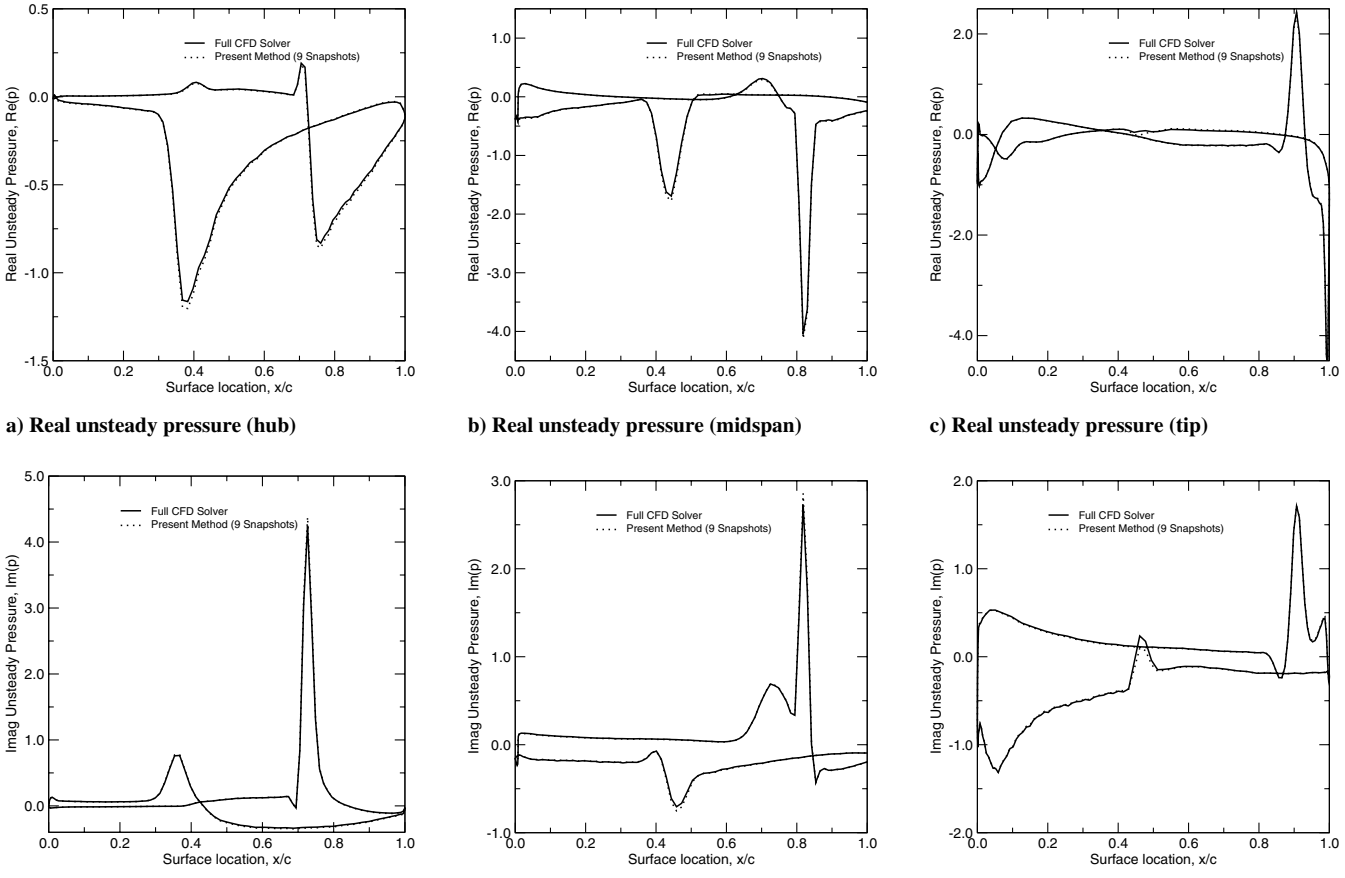

a) Real unsteady pressure (hub) **b) Real unsteady pressure (midspan)** **c) Real unsteady pressure (tip)**

d) Imag unsteady pressure (hub) **e) Imag unsteady pressure (midspan)** **f) Imag unsteady pressure (tip)**

Fig. 8 Comparison of unsteady pressure distribution of the front stage compressor blade computed using the present model and full CFD model. The rotor blades vibrate in first bending with $\sigma = 60$ deg.

or thirteen different interblade phase angles. The unsteady solutions were then computed using the resulting three sets of basis vectors over the full range of interblade phase angles. Shown in Fig. 6 are the real and the imaginary parts of the unsteady moment computed using the present technique with seven, nine, or thirteen vectors, as well as the unsteady moment computed using the full CFD solver. It can be seen that overall the present technique is in good agreement with the full CFD model. For seven snapshots, the behavior in the cut-on region cannot be predicted accurately, although rest of the interblade phase angle in the cut-off region is predicted quite accurately. For nine and thirteen snapshots the predicted unsteady solution is in excellent agreement with the time-linearized CFD solver for all interblade phase angles.

Finally, we investigate the error associated with the present technique. The procedure is straightforward. Once an approximate solution has been computed, we load this solution into our baseline CFD solver and compute residual by executing one iteration of the solver. As an example, Fig. 7a shows the solution residual for three different cases, that is, approximate solutions computed using seven, nine, and 13 snapshots. The first thing to note is that for interblade phase angles corresponding to a snapshot, the residual is very nearly zero. This is to be expected because the POD modes span the space of the solution at these points. Second, as the number of snapshots are increased, the average residual over the full range of interblade phase angles is reduced. For seven snapshots, the residual is well above 10^{-5} (our convergence criterion) for interblade phase angles in the region between -45 and 15 deg indicating more snapshots are needed to achieve our desired level of accuracy. For nine and 13 snapshots, the residuals for all interblade phase angles are below our threshold criterion (see Fig. 6).

In our method, the minimum number of snapshots needed for accurate answers is not known a priori, but an estimate of the error can be computed a posteriori. This naturally suggests the following strategy. We first estimate the unsteady solutions using a small number of snapshots (typically six), and check the residual at all interblade phase angles. If the error at any interblade phase angle exceeds our threshold, we then add one or more additional snapshots computed at or near interblade phase angles with large errors. As an example, we start with six equally spaced snapshot solutions and obtain estimates for the rest of the interblade phase angles. The residual for this case is shown in Fig. 7b. As can be seen, there are three points (-29, -14, and 6 deg) where the residual plot have peaks. In the next step, we compute snapshot solutions at these three interblade phase angles using our CFD solver. Those new snapshots are then included in our basis set and approximate solutions are again computed for the rest of the interblade phase angles. As one can see in

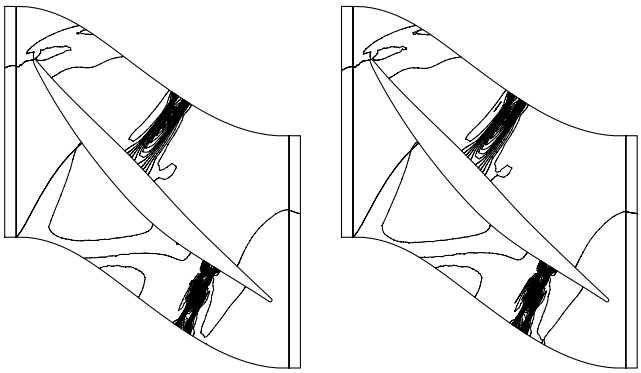

a) Time-linearized CFD solution **b) Estimated solution using the POD technique**

Fig. 9 Real part of computed and estimated unsteady pressure contours for the front stage compressor.

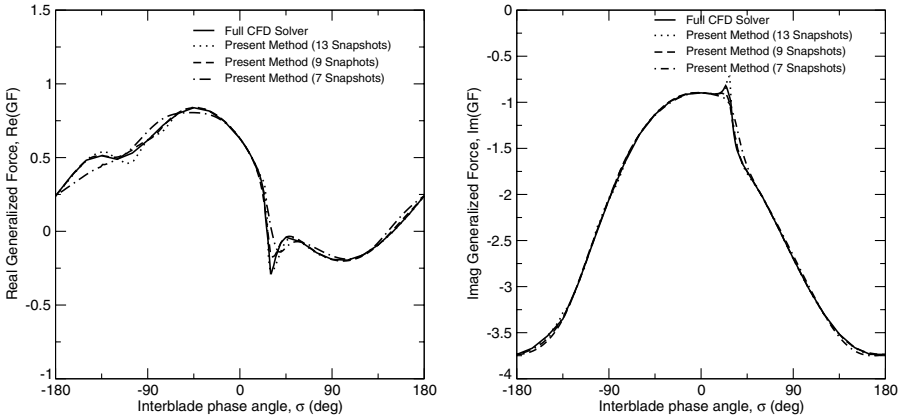

Fig. 10 Real and imaginary generalized force computed using the current technique and the full time-linearized CFD solver.

Fig. 7b, the error peaks are reduced, and the error levels are below our error threshold for all interblade phase angles.

Flutter Analysis of a Three-Dimensional Blade

To further illustrate the accuracy of the method, consider a three-dimensional rotor blade typical of those used in the front stage of a modern compressor. We consider here flow though the compressor row near the design point. The computational grid contains 51,731 points with 17 points in the radial direction. Although not shown here, a grid sensitivity study similar to the one presented in the previous case was performed to insure the computed solutions are grid converged. The flow conditions (total pressure, total temperature, flow angles) are prescribed at the inlet, and the static pressure is prescribed at the exit of the rotor. Using the time-linearized approach, one must first compute the steady flow through the blade row. Note that the flow for this configuration is transonic on the outer portion of the blade, with a shock impinging on the suction and the pressure sides of the blade.

Next, the blades of the compressor are assumed to vibrate in their first bending mode and frequency. The first step in the model is to compute the unsteady flow at several interblade phase angles using the conventional time-linearized flow solver. As in the previous test case, a total of nine snapshots are computed over a range of interblade phase angles. Eight of these nine snapshots are equally spaced over the possible range of interblade phase angles (i.e., every 45 deg), and the ninth snapshot is at 5 deg where the unsteady waves are cut-on. All of these snapshots are used to form nine basis vectors using the POD technique described in this note.

Having constructed the basis vectors, we compute an estimate of the unsteady solution at many interblade phase angles using the present fast approximate solution technique. As an example, consider the case of $\sigma = 60$ deg. This interblade phase angle is not a member of the original snapshot solutions. Figure 8 shows the computed real and imaginary parts of the unsteady surface pressure at three different spanwise locations (hub, midspan, and tip) of the blade for 60 deg. These results were computed using the present technique and, for comparison, the unmodified CFD scheme. As can be seen, the agreement between the present method and the full CFD computation is very good, despite using just nine snapshots in the model. Next we compare the real part of the unsteady pressure contours at the midspan section for the time-linearized CFD solver and the current POD method. As one can see from Fig. 9 our method is in very good agreement with the unsteady CFD solution.

The unsteady pressure distribution can be integrated to obtain the complex unsteady generalized force acting on the rotor blades due to their vibration. For this case, a negative imaginary part of the generalized force corresponds to a positive aerodynamic damping or a stable blade motion at a given interblade phase angle.

To investigate the effect of number of snapshots on accuracy, we computed basis vectors using seven, nine, or thirteen different interblade phase angles. The unsteady solutions were then computed using the resulting three reduced-order models over the full range of interblade phase angles with a spacing of 2 deg. Shown in Fig. 10 are the real and the imaginary parts of the generalized force computed using the present model with seven, nine, or thirteen vectors, as well as the generalized force computed using the full CFD solver. It can be seen that overall our technique is in good agreement with the full CFD model. For seven snapshots, some minor details cannot be captured between $\sigma = 0$ deg and 45 deg, although rest of the interblade phase angle values are predicted quite accurately. Within this interblade phase angle range, a so-called acoustic resonance occurs, with a characteristically abrupt change in the solution. However, when nine or 13 snapshots are used, the results of the full CFD solution can be reproduced with very high accuracy everywhere using the present technique. Although not shown here, the error estimation method used in the previous case was also performed for this case, with very similar results.

Conclusions

In this note, we have presented a technique for approximating the unsteady aerodynamic response of three-dimensional turbomachinery blades at many different interblade phase angles. The method, which is particularly well suited for the computation of the aerodynamic forces that produce flutter in turbomachinery, is computationally very efficient. The main computational cost of the method is the determination of a handful of snapshot solutions. Once these solutions are obtained, the rest of the unsteady solutions can be predicted with very little additional computational cost. The method is simple to implement, and can be retrofit to existing time-linearized flow solvers. Finally, error estimates can be computed a posteriori to determine the accuracy of the approximate solutions.

References

[1] Dowell, E. H., Hall, K. C., Thomas, J. P., Florea, R., Epureanu, B. I., and Heeg, J., "Reduced Order Models in Unsteady Aerodynamics," AIAA Paper 99-1261, 1999.

[2] Romanowski, M. C., and Dowell, E. H., "Reduced Order Euler Equations for Unsteady Aerodynamic Flows: Numerical Techniques," AIAA Paper 96-0528, Jan. 1996.

[3] Florea, R., and Hall, K. C., "Eigenmode Analysis of Unsteady Flows About Airfoils," *Journal of Computational Physics*, Vol. 147, No. 2, Dec. 1998, pp. 568–593.

[4] Kim, T., "Frequency-Domain Karhunen Loeve Method and Its Application to Linear Dynamic Systems," *AIAA Journal*, Vol. 36, No. 11, Nov. 1998, pp. 2117–2123.

[5] Hall, K. C., Thomas, J. P., and Dowell, E. H., "Proper Orthogonal Decomposition Technique for Transonic Unsteady Aerodynamic Flows," *AIAA Journal*, Vol. 38, No. 10, Oct. 2000, pp. 1853–1862.

[6] Willcox, K. E., Paduano, J. D., Peraire, J., and Hall, K. C., "Low Order Aerodynamic Models for Aeroelastic Control of Turbomachines," AIAA Paper 99-1467, 1999.

[7] Cizmas, P. G. A., and Palacios, A., "Proper Orthogonal Decomposition of Turbine Rotor-Stator Interaction," *Journal of Propulsion and Power*, Vol. 19, No. 2, Mar.–Apr. 2003, pp. 268–281.

[8] Lucia, D. J., Beran, P. S., and Silva, W. A., "Reduced-Order Modeling: New Approaches for Computational Physics," *Progress in Aerospace Sciences*, Vol. 40, No. 1–2, Feb. 2004, pp. 51–117.

[9] Epureanu, B. I., Hall, K. C., and Dowell, E. H., "Reduced-Order Models of Unsteady Viscous Flows in Turbomachinery Using Viscous-Inviscid Coupling," *Journal of Fluids and Structures*, Vol. 15, No. 2, Feb. 2001, pp. 255–273.

[10] Hall, K. C., and Ekici, K., "Multistage Coupling for Unsteady Flows in Turbomachinery," *AIAA Journal*, Vol. 43, No. 3, March 2005, pp. 624–632.

[11] Silkowski, P. D., and Hall, K. C., "A Coupled Mode Analysis of Unsteady Multistage Flows in Turbomachinery," *Journal of Turbomachinery*, Vol. 120, No. 3, July 1998, pp. 410–421.

[12] Ekici, K., Voytovych, D. M., and Hall, K. C., "Time-Linearized Navier–Stokes Analysis of Flutter in Multistage Turbomachines," AIAA Paper 2005-0836, 2005.

R. So
Associate Editor